



INSTITUT DE FRANCE
Académie des sciences

Comptes Rendus

Physique

Lionel Gélébart

Grain size effects and weakest link theory in 3D crystal plasticity simulations of polycrystals


Volume 22, issue S3 (2021), p. 313-330

<https://doi.org/10.5802/crphys.53>

Part of the Special Issue: Plasticity and Solid State Physics

Guest editors: Samuel Forest (Mines ParisTech, Université PSL, CNRS, France)
and David Rodney (Université Claude Bernard Lyon 1, France)

© Académie des sciences, Paris and the authors, 2021.
Some rights reserved.

 This article is licensed under the
CREATIVE COMMONS ATTRIBUTION 4.0 INTERNATIONAL LICENSE.
<http://creativecommons.org/licenses/by/4.0/>



*Les Comptes Rendus. Physique sont membres du
Centre Mersenne pour l'édition scientifique ouverte*
www.centre-mersenne.org



Grain size effects and weakest link theory in 3D crystal plasticity simulations of polycrystals

Lionel Gélébart[Ⓢ] ^a

^a Université Paris-Saclay, CEA, Service de Recherches Métallurgiques Appliquées,
91191, Gif-sur-Yvette, France
E-mail: lionel.gelebart@cea.fr

Abstract. The weakest link theory, sometimes proposed to analyze size effects on the plastic behaviour of single crystals, is introduced in 3D numerical simulations of polycrystals. The approach relies on a random distribution of sources in space and strength associated to a crystal plasticity law with constant per layer Critical Resolved Shear Stresses (CRSS). It is able to reproduce: (1) the grain size dependence of the yield stress given by the Hall–Petch law, (2) intense slip band localization patterns as often observed at the grains surface, especially pronounced in quenched or irradiated metals, but difficult to reproduce by numerical simulation.

Keywords. Weibull, Weakest link, Crystal plasticity, Size effect, Hall–Petch, Plastic strain localization, FFT.
Available online 3rd March 2021

1. Introduction

The present note lies in the context of the numerical simulation of polycrystals in the framework of continuum mechanics using the Finite Element method associated to Crystal Plasticity for the constitutive non-linear behaviour. Such simulations are now widely used by the “mechanics of materials” community focusing on polycrystalline materials. However, these simulations still suffer from different drawbacks when comparing numerical results with experimental ones.

The first one concerns the grain size sensitivity of the plastic behaviour of polycrystals, and more specifically of the yield stress that increases with decreasing grain sizes. This macroscopic evidence is well known since the early years of metallurgy. More recently, with the development of micro-machining and micro-testing, similar conclusions have been drawn on single crystals: the smaller the sample size, the higher the yield stress. Using “local” Crystal Plasticity, the stress is related to the strains which are dimensionless quantities, so that the numerical simulation result is independent of the size (the grain size for polycrystals or the sample size for single crystals). In that case the only way to incorporate size effects is to implement size dependent Critical Resolved Shear Stresses (CRSS) [1] or hardening parameters [2], whether homogeneously [2] or as a function of the distance from interfaces [3]. Alternatively, enhanced versions of crystal plasticity,

such as non-local crystal plasticity [4] or variants of Dislocation Field Mechanics [5] have been proposed to introduce size effects in the simulation of polycrystals [6, 7]. These models essentially take into account an additional hardening arising from the gradients of the plastic deformation through the dislocation density tensor.

A second drawback of “local” crystal plasticity in polycrystalline simulations concerns its ability to reproduce the plastic strain heterogeneity experimentally observed at the surface of polycrystals. Actually, the surface of the grains often exhibit slip traces, which are crossing entire grains. These traces can be characterized through Atomic Force Microscopy [8] or High Resolution Digital Image Correlation [9, 10] and an important challenge for the numerical simulation is to reproduce such plastic strain localization bands, especially enhanced in quenched or irradiated materials [11–13]. Using softening crystal plasticity is an efficient way to develop localization bands in simulations, however it has been demonstrated that two kinds of bands systematically appear, slip bands and kink bands, which is not consistent with most of the experiments in which intense localized slip bands dominate [11]. The combination of non-local and softening crystal plasticity has been recently explored [14] and proves to be an efficient way to promote slip band localization. Another approach consists in predefining, a priori, a set of geometrical slip bands (band parallel to slip planes) and assign them different plastic properties [15]. This methodology applied in the context of irradiated materials [12], exhibited an important kinematic hardening induced by a more realistic slip band network.

The present work consists of using “local” crystal plasticity and to introduce stochastic Critical Resolved Shear Stresses (CRSS) assigned to geometrical slip bands in 3D polycrystalline simulations. The goal and originality of this modelling is twice: introducing size effects (sample size or grain size) and generating more realistic plastic strain localization networks.

Taking into account the stochastic distribution of CRSS through the weakest link theory is an efficient way to introduce size effects. The idea is mentioned in the review of Papanikolaou [16], referring to analytical models [17, 18] and Dislocation Dynamic simulations [19–21]. However, both analytical and DD models suffer from a rough description of grains to grains interactions arising within a 3D polycrystal. The present work is then a first attempt to introduce the concept of stochastic distribution of CRSS within 3D polycrystalline simulations in order to investigate its influence on both the macroscopic behaviour and the local strain fields.

Section 2 introduces the weakest link model proposed for crystal plasticity in a simple 1D case of a single crystal submitted to simple shear (one slip system). Extensions of this model to 3D numerical simulations are proposed in Section 3. Sections 4 and 5 illustrate their capabilities in terms of macroscopic behaviour and plastic strain distribution through the simulations of both FCC single and poly-crystals. Discussion, conclusion and future prospects are proposed in Section 6.

2. The weakest link model for 1D crystal plasticity (single crystal, single slip)

The simple 1D model considers a parallelepiped sample Ω of volume V , submitted to a shear stress $\bar{\tau}$. The material is a single crystal with a single slip system favourably oriented. Dislocation sources are assumed randomly distributed in space together with a random distribution of CRSS τ . Then, dislocation sources are considered as punctual flaws, corresponding to random points (x, τ) in the *flaw space* $\Omega \times]0, \infty[$, so that the flaw population is a point process in the flaw space. Assuming that the flaws are independent, their distribution corresponds to a Poisson point process.

The link between the Poisson point process and the commonly used Weibull model can be found in [22, Section 2.1] with in mind the analogy between plasticity and brittle failure: the source strength (or CRSS) for plasticity corresponding to the flaw strength for brittle failure, the

sample deforms plastically if the applied stress reaches the lowest CRSS present in the volume. Therefore, according to the Weibull model, the probability that the sample remains elastic reads:

$$P(\bar{\tau}) = P\{N(\Omega \times]0, \bar{\tau}[) = 0\} = \exp\left(-\frac{V}{V_0} \left(\frac{\bar{\tau}}{\tau_0}\right)^m\right) = \exp\left(-\left(\frac{\bar{\tau}}{\lambda}\right)^m\right) \quad (1)$$

where $N(\Omega \times]0, \bar{\tau}[)$ is the number of flaws in the domain $(\Omega \times]0, \bar{\tau}[)$ of the flaw space, and consequently, $P\{N(\Omega \times]0, \bar{\tau}[) = 0\}$ is the probability to find zero flaw in the same domain (i.e. so that the sample remains elastic). Note that the probability that a sample deforms plastically is then $F = 1 - P$, which is the cumulative distribution function of the Weibull distribution. The two parameters of the model are m and τ_0 , with V_0 an arbitrary reference volume (generally 1 m^3). Used in the following, λ is a volume dependent parameter according to $\lambda = \tau_0(V_0/V)^{1/m}$.

It can clearly be observed that F (or P) depends on the volume V : F decreases when the volume decreases. Hence, the smaller the volume the lower the probability that the sample deforms plastically, or in other words, smaller is stronger. In addition, for a given couple of parameter m and τ_0 , the median, the mean and the standard deviation of the Weibull distribution, are proportional to the parameter λ and consequently to $V^{-1/m}$ so that they all decrease when the volume increases.

The generation of a random set of values satisfying the Weibull model (Equation (1)) follows the method used in [22] (Section 3.1, citing [23]). Let U a set of random variables uniformly distributed in $[0, 1]$, then a random set of CRSS satisfying (Equation (1)) is simply obtained by applying to U the inverse of the function $P(\bar{\tau})$:

$$\tau_c = \tau_0 \left(-\frac{\ln(U)V_0}{V}\right)^{\frac{1}{m}} \quad (2)$$

The weakest link model is well suited to analyse results obtained on single crystalline samples submitted to micro-tensile (or compression) tests, whether experimentally [19] or numerically with Dislocation Dynamics [19,20]. The extension of this idea to the size-dependent macroscopic yield stress of 3D polycrystals seems promising but is not straightforward. Actually, starting from an initial homogeneous stress field, following the weakest link assumption, as soon as the first grain deforms plastically the complete polycrystal should also deform plastically. However, the first sign of plasticity is quite different from the macroscopic plastic flow, which comes with the plastic deformation of a large number of grains. Then a direct application of the weakest link to the whole polycrystal is not suitable to describe the macroscopic yield stress. Besides, as soon as plasticity occurs in the first grain, the stress field becomes heterogeneous and grain to grain interactions have to be taken into account. This can be done classically with 3D numerical simulations accounting for crystal plasticity, but it raises the question of representing the variability (location and CRSS) associated to dislocation sources within grains.

3. Extension to 3D numerical simulations

The numerical simulations described in this work have been performed with the FFT-based solver AMITEX_FFTP [24] based on linear hexahedral finite elements with reduced integration [25]. The input geometry is a 3D digital image (i.e. a regular grid of voxels), each voxel corresponding to a hexahedral finite element, with stress and strain evaluated at centres, and displacement and stress divergence evaluated at nodes. The crystal plasticity behaviour law is implemented through the MFRONT code generator [26], compatible with AMITEX_FFTP. The numerical integration of quasi-perfect crystal plasticity being numerically heavy, the simulations take benefit from the MPI parallel distributed memory implementation.

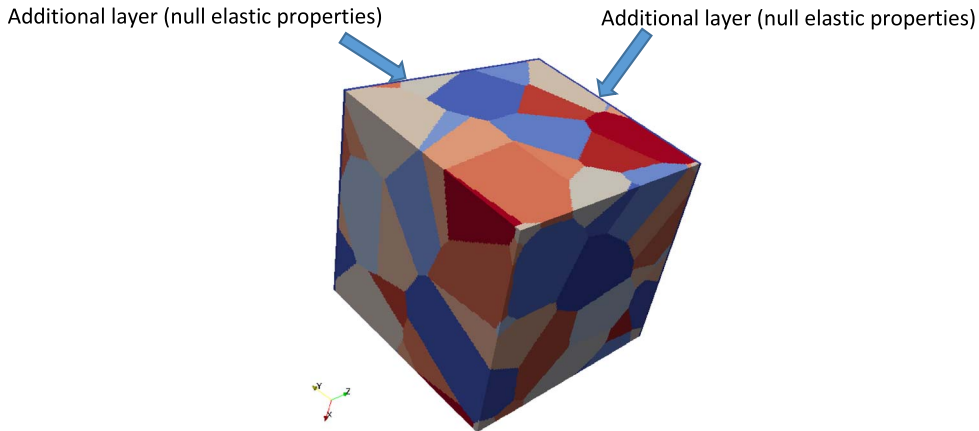


Figure 1. Unit-cell with 27 grains polycrystal and additional layers (two voxels thickness) of voxels with null elastic properties to apply stress free boundary conditions on Y - and Z -faces. Periodic BC are applied on X -faces.

3.1. Geometry, loading and behaviour law

3.1.1. Single and poly-crystals tensile test

Both single and poly-crystals, represented by cubic unit-cells, are submitted to a tensile test loading in the X direction. The macroscopic strain is applied with a strain rate of 10^{-4} s^{-1} up to a plastic strain of 1%, with an interruption at 0.2% of plastic strain to store the cumulated plastic strain fields (Equation (6)). Using a FFT-based solver, periodicity is assumed between X -faces. In order to relax periodic Boundary Conditions and apply stress free BC, additional layers (two voxel thickness) with null elastic properties are added on Y -faces and Z -faces (see Figure 1). Note that there is no need to use more than two voxels to mimic free surfaces (in practice a single voxel would have been sufficient as the AMITEX_FFTP code is equivalent to the use of linear hexahedral finite elements with reduced integration).

For the single crystal, three sample sizes have been considered, $D = 1 \mu\text{m}$, $10 \mu\text{m}$ and $100 \mu\text{m}$, and two grid refinements have been used $n_x = 50$ and 100 . The spatial resolution is $\delta x = D/n_x$ and the volume of a voxel is $\delta V = (\delta x)^3$. For the polycrystal, the unit-cell consists of 27 grains generated by a Voronoï tessellation technique based on a random (uniform) distribution of 27 seeds and assuming periodicity of the microstructure (see Figure 1). Four average grain sizes have been considered, $D_g = 1 \mu\text{m}$, $3 \mu\text{m}$, $10 \mu\text{m}$ and $100 \mu\text{m}$, corresponding to unit-cell sizes of $3 \mu\text{m}$, $9 \mu\text{m}$, $30 \mu\text{m}$ and $300 \mu\text{m}$ for the 27 (i.e. $3 \times 3 \times 3$) grains. Defining the grid refinement n_x as the number of voxels per length D_g , the 27 grains unit-cell is discretised in grids of $150 \times 150 \times 150$ voxels for $n_x = 50$, and $300 \times 300 \times 300$ voxels for $n_x = 100$. The spatial resolution is $\delta x = D_g/n_x$ and the volume of a voxel is $\delta V = (\delta x)^3$.

3.1.2. Crystal plasticity

As a first attempt, the use of a simple quasi-perfect crystal plasticity law allows to evaluate the effect of the CRSS spatial distribution (described in Section 3.2), independently from any other local hardening contribution. Then, focusing on the onset of plasticity (i.e. the maximum macroscopic plastic strain is 1%), the small strains assumption is used in the modelling. The

corresponding constitutive equations are given below.

$$\underline{\sigma} = \mathbf{C}: (\underline{\varepsilon} - \underline{\varepsilon}^P) \quad (3)$$

$$\dot{\underline{\varepsilon}}^P = \sum_{s=1}^N \dot{\gamma}_s \underline{\mu}_s \quad (4)$$

$$\dot{\gamma}_s = \text{sign}(\tau_s) \left(\frac{|\tau_s| - (\tau_P + \tau_s^f)}{K} \right)_+^n \quad (5)$$

The elasticity, Equation (3), is assumed isotropic with a Young modulus and Poisson coefficient of 110 GPa and 0.3, respectively. The shear stress τ_s on system s is $\tau_s = \underline{\sigma} : \underline{\mu}_s$ with $\underline{\mu}_s = (m_s \otimes n_s)^{\text{sym}}$, m_s and n_s being the slip direction and normal to slip plane direction. The plastic strain rate, Equation (4), is given by the sum of the slip contributions over the systems. The slip systems accounted for in the simulations are the 12 slip systems of type $\{111\}\langle 1\bar{1}0\rangle$, commonly observed in FCC crystallographic phases. Finally, for each system, the shear strain rate is governed by the Norton rule with parameter K and exponent n . The expression $(X)_+$, is equal to X if positive and zero otherwise. The CRSS required to activate plasticity is then $\tau_P + \tau_s^f$, where τ_P is homogeneous and τ_s^f denotes heterogeneous (fluctuating) fields introducing the variability associated to dislocations sources (position and strength) within grains. There is one field per slip system, 12 in the present case, and their description is detailed in the next section. The constant value τ_P is attributed to the Peierls stress (or lattice friction stress) required to move dislocations. This parameter is rather small for FCC crystals and an average value of 5 MPa is chosen (values between 0.3 MPa and 9 MPa for different FCC materials in [27]). Finally the choice of the Norton law parameters, (10 MPa, 4) for (K, n) , results from a compromise between numerical efficiency and the proximity with perfect plasticity. In practice, the Norton exponent of 4 is standard when considering viscoplasticity and dislocation creep. Then, the K parameter has been adjusted to reduce the viscous effect (less than +/1% relative difference on the macroscopic uniaxial stress at 2% strain for strain rates between 10^{-3} s^{-1} and 10^{-2} s^{-1}).

The cumulated plastic strain field is output from simulations as it represents in a single scalar field the plastic strain activity. Its rate definition reads:

$$\dot{p} = \sqrt{\dot{\underline{\varepsilon}}^P : \dot{\underline{\varepsilon}}^P}. \quad (6)$$

3.2. CRSS distribution

The purpose of this section is to generate 3D random fields τ_s^f , used in (5), in relation with the Poisson point process introduced in Section 2 leading to the Weibull model described by (1).

3.2.1. Per voxel distribution

A first attempt consists in using for generating the $(N_x)^3$ values (one value per voxel) of τ_s^f , the same Weibull distribution as given in (1), with the volume V replaced by δV , the voxel volume. Then, the evaluation of the $(N_x)^3$ random values comes directly from (2), with $V = \delta V$. A field τ_s^f , see Figure 2 (left), is then an image of the lowest source strength (for system s) within each voxel, assuming sources as points randomly distributed in space and strength according to a Poisson point process. Hence, the simulation should initiate at the voxels where τ_s^f is the lowest.

However, the problem with this description, used in combination with a local crystal plasticity model (here, Equations (3)–(5)), is that when plasticity initiates in a voxel x_o for system s (i.e. the shear stress τ_s reaches $\tau_P + \tau_s^f(x_o)$), it is not able to freely propagate in the surrounding voxels crossed by the same gliding plane because their fluctuating CRSS τ_s^f can be much higher than $\tau_s^f(x_o)$.

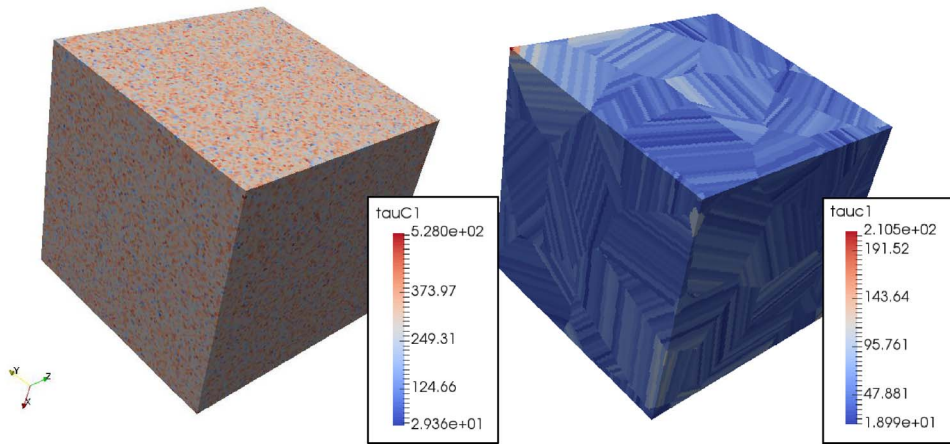


Figure 2. Per-voxel random distribution of τ_s^f for a voxel size of $\delta x = 0.1 \mu\text{m}$ and a $100 \times 100 \times 100$ unit-cell (left). Per-layer random distribution of τ_s^f for a grain size $D_g = 10 \mu\text{m}$ and a refinement $n_x = 50$ (right). In both case, there is one random field per slip system so that 12 different fields are considered in the complete model.

3.2.2. Per layer distribution

In order to circumvent the issue suspected with the per voxel distribution, while keeping a local crystal plasticity model, the idea is to define (in each grain) thin layers parallel to the slip plane of system s and assign a constant τ value for the voxels of a same layer as displayed on Figure 2 (right). To assign the per-layer values, two methods can be used. The first one, consists in using the field τ_s^f defined per voxel just above and to assign the minimum value present in the layer to the whole layer. The second method has not been used but should be statistically equivalent. It consists in following the Weibull model of (1) with the volume of the layers (indexed i) and use (2), with $V = V_{\text{layer}_i}$, to define one random value per layer. The field τ_s^f is now an image of the lowest source strength within each layer. As twelve systems are considered, twelve different fields have to be generated as inputs of the numerical simulation (it was also the case for the per voxel approach).

With that description, if plasticity initiates in a layer, it should be able to propagate and cross the entire grain, letting a straight slip trace at the surface as often observed experimentally. As a counterpart, using a per-layer constant value we lose the position of the weakest source whose strength is affected to the complete layer. In addition, the layer thickness becomes an additional material parameter.

Note finally that the two distributions rely on the same Weibull model (Equation (1)), built on the same random point Poisson process for the distribution of sources. They differ from the volumes which are considered in the model, the volume of the voxels δV in the first case, and the volume of the layers V_{layer_i} in the second case.

3.2.3. Weibull parameters

As a first exploration of the model, the couple of Weibull parameters (τ_0, m) is set to (0.1063 MPa, 6). The choice of the exponent m derives from the following simplified analysis. The median value of a Weibull distribution (Equation (1)) being $M_d = \lambda(\ln 2)^{1/m} = \tau_0(\ln 2 \cdot (V_0/V_d))^{1/m}$, with V_d the volume of a grain of diameter d , then $M_d \propto d^{-3/m}$. Assuming that the grain size dependent part of the classical Hall–Petch relation $\sigma^y = \sigma^0 + kd^{-1/2}$ is proportional to M_d , then m

should take the value of 6. Whatever the simplicity of the reasoning, this value lies in the range of experimental values (between 4 and 20 in [28]).

The second Weibull parameters $\tau_0 = 0.1063$ MPa, corresponds to an arbitrary choice for the median value $M_{1 \mu\text{m}}$ of 100 MPa for a volume of $1 \mu\text{m}^3$ (see Section 2).

3.3. Post-treatment: yield stress definitions

The definition of the macroscopic yield stress is conventionally defined on tensile test stress–strain curves as the stress $\sigma_{0.2\%}^y$ for which the plastic strain is 0.2%. This definition, together with $\sigma_{1\%}^y$, the yield stress for 1% plastic strain, are used to investigate size effects (sample size or grain size) on the macroscopic plastic behaviour of the unit-cell.

However, these yield stresses essentially characterize the stress for which the plastic flow is significant from a macroscopic point of view. Conversely, it is also of interest to evaluate the yield stress corresponding to the first signs of plasticity. For that purpose, we define $\sigma_{0\%}^y$ as the stress corresponding to the detection of the first non-linearity. In practice, $\sigma_{0\%}^y$ is extracted from the simulated stress–strain curves as the lowest value for which the ratio (tangent modulus/secant modulus) is below 0.999.

4. Single crystal cubic unit-cell

The single crystal is submitted to a tensile test loading in the (100) direction of the FCC crystal, so that, from the loading point of view, 8 slip systems have the same maximum Schmid factor ($1/\sqrt{6} = 0.4082$). However, from the CRSS point of view, considering one stochastic field per slip system, the CRSS are different for the 12 slip systems. This section is a first step towards the 3D polycrystal simulation, its main purposes are: first, demonstrating from numerical results that the “per voxel distribution” strategy is not suitable, and second, validating the “per layer distribution” strategy by comparing numerical results with the results expected from the Weibull model.

4.1. Per voxel distribution

For each sample size D and refinement n_x , 3 different random realizations of the 12 fluctuating CRSS fields τ_s^f have been generated and used as input of the simulations. With 3 sample sizes and 2 refinements, 18 simulations have been performed.

Both the macroscopic behaviour and the local plastic strain fields are reported on Figure 3. From the macroscopic point of view, the behaviour exhibits, as expected, a sample size dependence: for a given grid refinement the higher the sample size the lower the yield stress. Note that in spite of random CRSS fields, the three simulations performed for each configuration (sample size, refinement), exhibit almost superimposed stress–strain curves. On the other hand, the behaviour exhibits a very important and undesired dependence with respect to the spatial resolution δx . Actually, using the Weibull model of (1) with $V = \delta V$ modifies the distribution towards higher values when decreasing δV , as observed on the median value $M = \tau_0 (\ln 2 \cdot (V_0/\delta V))^{1/m}$. However, in the 3D numerical simulation the weakest link theory is not reproduced: the sample do not deform plastically as soon as a first voxel deforms plastically but it requires a large enough amount of voxels, with higher CRSS, to deform which hardens the behaviour.

Finally, the distribution of the cumulated plastic strain, Figure 3 (right), is quite noisy and does not exhibit slip band localizations crossing the sample as it can be observed when experimentally testing single crystals for example with micro-pillars.

As a conclusion, per voxel distributions of CRSS are not convenient to introduce the idea of randomly distributed sources in 3D crystal plasticity numerical simulations.

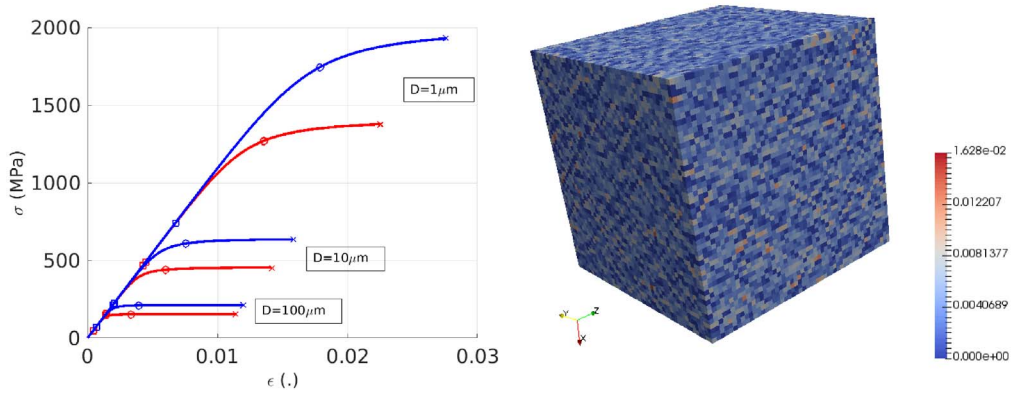


Figure 3. Single crystal unit-cell with per voxel CRSS random fields. On the left, the stress–strain curves obtained for different sample sizes ($D = 1 \mu\text{m}$, $10 \mu\text{m}$ and $100 \mu\text{m}$) and two grid refinements, $n_x = 50$ and $n_x = 100$, respectively in red and blue. For each configuration (sample size, grid refinement) three simulations results, obtained with three different random realizations of CRSS fluctuating fields, are almost perfectly superimposed. On the right, example of a spatial distribution of the cumulated plastic strain (after 0.2% plastic strain).

4.2. Per layer distribution

In this study, the layer thickness e is arbitrarily related to the spatial resolution δx so that two voxels represent the layer thickness (i.e. $e = 2\delta x$). As a consequence, for a given unit-cell size D , the layer thickness e decreases when increasing the refinement n_x (decreasing $\delta x = 2D/n_x$).

In addition to the 18 (3 realizations \times 3 sizes \times 2 refinements) simulations run up to a plastic strain of 1%, 7 additional random realizations have been generated to perform 42 ($7 \times 3 \times 2$) additional simulations up to 0.2% of plastic strain. This allows to account for the variability observed on the macroscopic response, with a focus on the yield stresses $\sigma_{0\%}^y$ and $\sigma_{0.2\%}^y$. Both the macroscopic behaviour and the local plastic strain fields are reported on Figure 4.

4.2.1. The onset of plasticity ($\sigma_{0\%}^y$)

The onset of plasticity is investigated through the analysis of $\sigma_{0\%}^y$ detecting the first signs of plasticity (see Section 3.3). In the elastic domain, the elastic behaviour being homogeneous, the stress field is uniform. Considering the Weibull model described in Section 2, but now with eight slip systems having the same Schmid factor ($1/\sqrt{6}$), the probability that the sample remains elastic is the product of the probabilities that plasticity is not reached on each slip systems. It is equivalent to consider a volume eight times larger in (1) so that the median value for the yield stress reads:

$$\overline{\sigma_{0\%}^y} = \left(\tau_P + \tau_0 \left(\ln 2 \cdot \frac{V_0}{8V} \right)^{\frac{1}{m}} \right) \sqrt{6} \quad (7)$$

The comparison with the post-treatment of 3D numerical simulations on ten samples is reported in Table 1. The fourth column in Table 1 comes from a pre-treatment of the random CRSS fields used in simulations: for each sample, $\sigma_{0\%}^y$ is evaluated from the minimum value of the CRSS fields for the 8 potential active slip systems. This value should be equal to the yield stress $\sigma_{0\%}^y$ detected from the simulated stress–strain curve in the third column. The slight difference, observed on the median, is attributed to the detection procedure and more specifically to the loading increment used in simulation. The slight difference between the two resolutions,

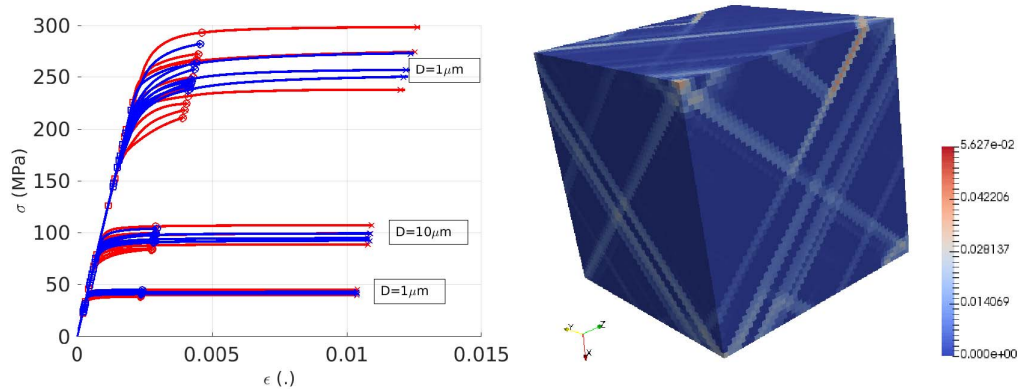


Figure 4. Single crystal unit-cell with per layer CRSS random fields. On the left, the stress–strain curves obtained for different sample sizes ($D = 1 \mu\text{m}$, $10 \mu\text{m}$ and $100 \mu\text{m}$) and two grid refinements, $n_x = 50$ and $n_x = 100$, respectively in red and blue. For each configuration (sample size, grid refinement) three simulations run up to 1% plastic strain and seven run up to 0.2%. On the right, example of a spatial distribution of the cumulated plastic strain (after 0.2% plastic strain).

Table 1. Evaluation of the median yield stress $\overline{\sigma_{0\%}^y}$ evaluated from the Weibull model, and from a post- and pre-treatment of ten 3D numerical simulations on single crystal cubic unit-cell

D (μm)	$\overline{\sigma_{0\%}^y}$ (Equation (7)) (MPa)	$\overline{\sigma_{0\%}^y}$ (post-treatment) (MPa)	$\overline{\sigma_{0\%}^y}$ (pre-treatment) (MPa)
1	185.5	181.6 / 172.3	188.4 / 180
10	67.0	62.3 / 62.3	68 / 65.3
100	29.6	28.4 / 28.0	29 / 29.9

Two values are given, one for each refinement, $n_x = 50$ and 100 .

also observed on the “pre-treatment” values, is attributed to the low number of samples as it (increasing the number of samples reduces the difference). Finally, the comparison of the numerical values (pre- and post-treatment) are in good agreement with the analytical model (Equation (7)). It validates, at least for the single crystal case, both the numerical method and its correct implementation.

4.2.2. Macroscopic plastic flow ($\sigma_{0.2\%}^y$)

As observed on Figure 4, the yield stresses at the onset of plasticity $\sigma_{0\%}^y$ reported in Table 1 are much lower than the yield stresses $\sigma_{0.2\%}^y$, for which the sample flows macroscopically, reported in Table 2. This important difference, which can be surprising for a single crystal, comes from the use of periodic boundary conditions in the axial direction together with the cubic geometry of the unit-cell. Actually, in a cubic cell, every $\{111\}$ planes in a cubic sample are intersecting the faces submitted to periodic boundary conditions. As the periodically repeated CRSS fields are not continuous when crossing these faces, a weak $\{111\}$ layer in the unit-cell does not coincide with a weak $\{111\}$ plane in the periodically repeated unit-cell so that it hinders the localization of plastic strain in the weakest layer. This interaction between neighbouring unit-cells induces an important hardening observed on the macroscopic curves (Figure 4, left) and the activation of various weak planes as observed on the plastic strain maps (Figure 4, right). A deeper analysis

Table 2. $\overline{\sigma_{0.2\%}^y}$ (median over 10 realizations) evaluated for the single crystal cubic unit-cell for different unit-cell size

D (μm)	$\overline{\sigma_{0.2\%}^y}$ (MPa)
1	245.3/246.9
10	91.9/93.4
100	41.1/41.9

Two values are given, one for each resolution, $n_x = 50$ and 100.

of the cumulated plastic strain field reveals that the four slip traces corresponding to the four $\{111\}$ slip planes are generally observed in these simulations. However, the plastic strain intensity strongly differs from one slip trace to another and the situation appears more complicated in the neighbourhood of the periodic boundaries (more slip traces with reduced intensity). As observed on Figure 4, it must also be noticed that an important part of the unit-cell remains almost plastically undeformed.

If the variability of $\sigma_{0.2\%}^y$ is almost negligible with the per voxel approach, here, it exhibits an important size effect: the higher the sample size the lower the variability (qualitatively observed on Figure 4). This effect is now consistent with the weakest link approach. In addition, the effect of the refinement $\overline{n_x}$, and consequently of the layer thickness (as $e = 2D/n_x$), is almost negligible as observed on $\overline{\sigma_{0.2\%}^y}$ in Table 2. Contrary to the per voxel approach, the per layer distribution allows for the propagation of plasticity as soon as it is initiated in a layer.

As a conclusion, the per layer approach proves to be much better suited to account for randomly distributed sources.

4.3. Main results

The main results deduced from simulations on a single crystal cubic unit-cell are summarized below:

- The per-voxel distribution approach suffers from an important mesh size dependence and an unexpected low variability. The problem comes from the fact that the weakest link theory cannot be represented in this approach as neighbouring voxels are interacting in the mechanical simulation (i.e. a voxel with a high CRSS may strongly interact with a neighbouring voxel with a low CRSS).
- The per-layer distribution of CRSS allows to overcome these issues. Actually, with a CRSS constant per layer, if plasticity is activated in a voxel it is not hindered by voxels lying in the slip plane with higher CRSS. A drawback of this approach is that the exact location of the critical source within the layer is lost.
- Because of the reduced size of the unit-cell in the axial direction, the effect of the boundary conditions is not negligible, it explains the difference between $\sigma_{0\%}^y$ (at the real onset of plasticity) directly related to the minimum CRSS in the unit-cell, and $\sigma_{0.2\%}^y$. Actually, the two periodic faces act as interfaces between the repeated unit-cells.

5. Polycrystal unit-cell

Following the main results obtained on the single crystal unit-cell, the per-voxel distribution approach is abandoned in the present section. Consistently with the previous study on the single crystal cubic unit-cell, the layer thickness is still related to the refinement n_x with the relation $e = 2\delta x = 2D_g/n_x$ (i.e. two voxels per layer thickness).

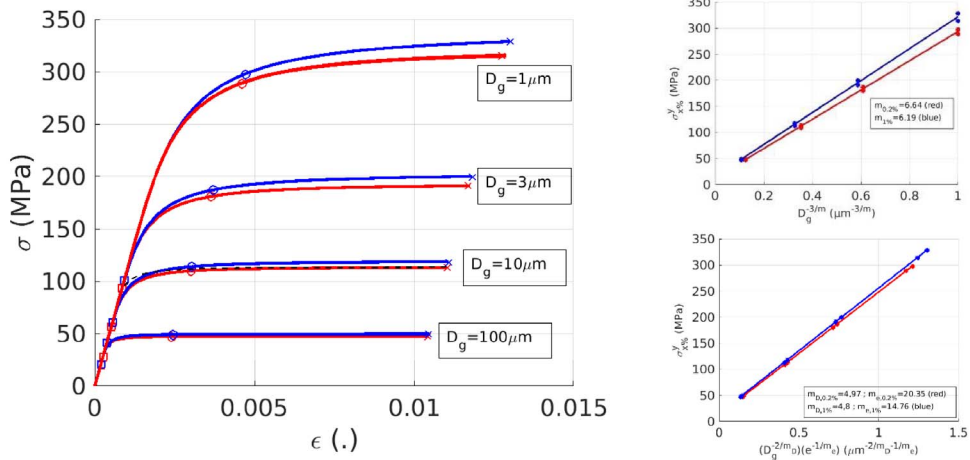


Figure 5. Polycrystal unit-cell with per layer CRSS random fields. Average stress/strain curves for the polycrystal unit-cell, for different grain sizes (left). In blue and red, for the grid resolutions $n_x = 100$ and 50 respectively. In thin black-dotted line, the curve obtained for $D_g = 10 \mu\text{m}$ and $n_x = 50$ with a homogeneous CRSS (adjusted on the red curve). Adjustment of two yield stress size dependent models (right), described by (8) (up) and (9) (down).

A single simulation is performed for each refinement n_x and grain size D_g , with a single random realization of the CRSS fields for each simulation. The variability is evaluated for the smaller grain size $D_g = 1 \mu\text{m}$ (and the refinement $n_x = 50$) with three different random realizations. Finally, for the sake of comparison, an additional simulation is performed, for the refinement $n_x = 50$, with the classical assumption of a homogeneous CRSS over the whole polycrystal.

Note the different underlying assumptions related to these simulations: plasticity is governed by sources located in the volume of the grains (i.e. not at the grain boundaries) and the Weibull parameters describing the source distribution are the same for all the grain sizes.

5.1. Macroscopic behaviour

On Figure 5 (left), the three different simulations performed for the smaller grain size $D_g = 1 \mu\text{m}$, are almost superimposed so that a single realization is representative of the macroscopic behavior. As observed on the single crystal in Section 4.2, the variability is suspected to increase with a decreasing grain size. Therefore, the single simulations performed for each of the two larger grain sizes are also representative. This is an interesting result: the variability observed on the macroscopic response of single crystal simulations, arising from the random distribution of CRSS introduced at the grain scale, completely disappears when simulating a polycrystal. This point is all the more striking as the number of grains, 27 , is reduced. It can be explained by the interactions resulting from grain boundary interfaces. For the single crystal cubic unit-cell the effect is reduced because the only interfaces limiting the propagation of plasticity through the whole sample are the X -faces submitted to periodic BC, the Y - and Z -surfaces being free surfaces. For the polycrystal unit-cell, the propagation of plasticity through the entire sample must cross an important number of grain boundary interfaces between the Y - and Z -free surfaces.

However, if variability has disappeared in spite of random CRSS fields, the grain size effect remains (Figure 5, left). To analyse the grain size dependence of the yield stress, a Hall–Petch like relation (Equation (8)) is proposed. For a given $x\%$ (0.2% or 1%), the three parameters

Table 3. Adjustment of the 3 parameters model (Equation (8)) describing the macroscopic yield stresses as a function of D_g

	$\sigma_{x\%}^0$ MPa	$k_{x\%}$ MPa (μm) $^{1/m_{x\%}}$	$m_{x\%}$
$x = 0.2\%$	13.0	280.5	6.64
$x = 1\%$	15.7	306.1	6.19

Table 4. Adjustment of the 4 parameters model (Equation (9)) describing the macroscopic yield stresses as a function of D_g and e

	$\sigma_{x\%}^0$ MPa	$k_{x\%}$ MPa (μm) $^{1/m_{x\%}}$	$m_{D_g, x\%}$	$m_{e, x\%}$
$x = 0.2\%$	12.9	235.4	4.97	20.35
$x = 1\%$	15.6	240.4	4.80	14.76

($\sigma_{x\%}^0, k_{x\%}, m_{x\%}$), adjusted on the 8 numerical yield stresses $\sigma_{x\%}^y$ (four grain size, two refinements), are reported in Table 3 (adjustment displayed on Figure 5, up right). It is noticeable that the resulting exponent $m_{x\%}$ is close to the m exponent of the Weibull distribution for the CRSS ($m = 6$), especially for the highest plastic strain (1%). Hence, as proposed in Section 3.2.3, the size dependent part of the yield stress follows approximately the same size dependence as the Weibull model's median : $M_{D_g} \propto D_g^{-3/m}$.

$$\sigma_{x\%}^y = \sigma_{x\%}^0 + k_{x\%} D_g^{-\frac{3}{m_{x\%}}} \quad (8)$$

The effect of the layer thickness e , resulting from the constraint $e = 2D_g/n_x$, is observed on the red and blue curves on Figure 5 (left), respectively with refinements $n_x = 50$ and $n_x = 100$. The effect is not negligible and can be explained as follows. When reducing the volume of the layers, the mean and median of the Weibull distribution increase, and consequently, the spatial average of the per layer CRSS fields increases. Note that this effect almost vanishes when considering a single crystal sample with stress free boundaries (see Section 4.2). A modified relation is proposed in (9) to dissociate the grain size and the layer thickness. The adjusted parameters are given in Table 4 and the better quality of the adjustment is observed on Figure 5 (right, down). With this model, for a given thickness, the size dependent part of $\sigma_{x\%}^y$ are $\propto D_g^{-1/2.5}$ and $\propto D_g^{-1/2.4}$, for $x\% = 0.2\%$ and 1% respectively.

$$\sigma_{x\%}^y = \sigma_{x\%}^0 + k_{x\%} D_g^{-\frac{2}{m_{D_g, x\%}}} e^{-\frac{1}{m_{e, x\%}}} \quad (9)$$

5.2. Plastic strain distribution

As a general remark from Figures 6–9, it must be emphasized that the cumulated plastic strain fields, obtained with the per layer CRSS distribution, are highly heterogeneous with very high values compared to the 0.2% macroscopic plastic strain. The plastic strain is localized in a few activated layers forming intragranular patterns. Qualitatively, it seems that, in general, two different $\{111\}$ planes are activated per grain, and sometimes, a single plane or three different planes are observed.

The negligible macroscopic variability observed in Section 5.1 is now discussed through the plastic strain fields displayed on Figure 6. The first noticeable point is that, for three realizations, the plastic strain localization patterns are different while the macroscopic stress is exactly the same. However, if the patterns are different, it seems, at least qualitatively, that the activated

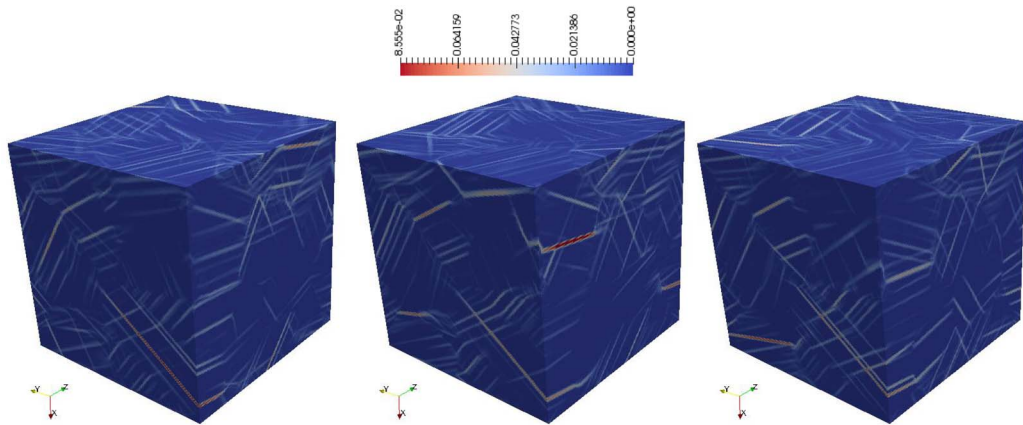


Figure 6. Polycrystal unit-cell—Cumulated plastic strain fields (at 0.2% macroscopic plastic strain) for three different random CRSS per layer distributions ($D_g = 1 \mu\text{m}$, $n_x = 50$). Colorbar is adjusted on the narrower data range.

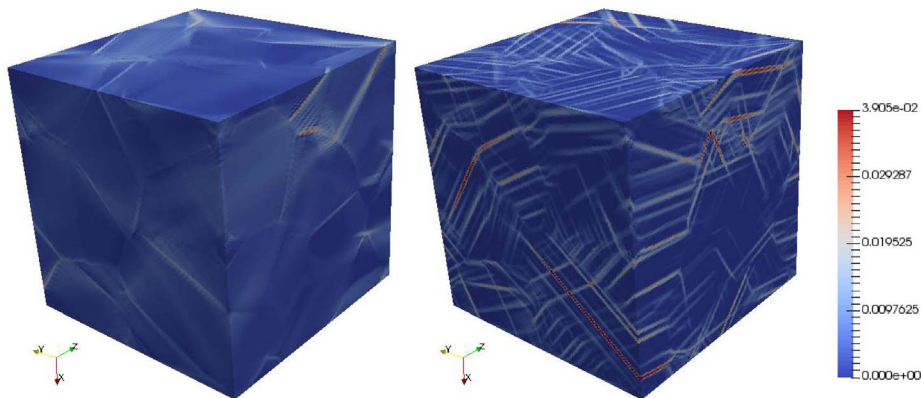


Figure 7. Polycrystal unit-cell—Cumulated plastic strain fields (at 0.2% macroscopic plastic strain), for homogeneous (left) and per layer random (right) distributions of CRSS ($D_g = 10 \mu\text{m}$, $n_x = 50$). Colorbar is adjusted to the homogeneous case data range.

{111} planes are often the same in the corresponding grains of the different simulations but with different locations and intensities.

The comparison between the homogeneous CRSS assumption and the present random description is performed, for the case ($D_g = 10 \mu\text{m}$, $n_x = 50$), after adjusting the homogeneous CRSS on the macroscopic behaviour obtained with the per layer distribution. The adjusted value is 38MPa and the corresponding curve is drawn in thin black dashed line on Figure 5. The plastic strain field on Figure 7 is far less localized than with the per layer distribution. To reinforce the localization and patterning in the case of homogeneous CRSS, softening crystal plasticity has been demonstrated in [11]. However, the refined analysis of the plastic strain fields revealed an important and systematic contribution of localized kink bands (perpendicular to the slip planes). This result was consistent with the bifurcation analysis of Asaro and Rice [29] but is not frequently observed in experiment. The per layer approach allows to prevent localized kink banding.

The influence of the grain size on the plastic strain fields is displayed on Figure 8: the higher the

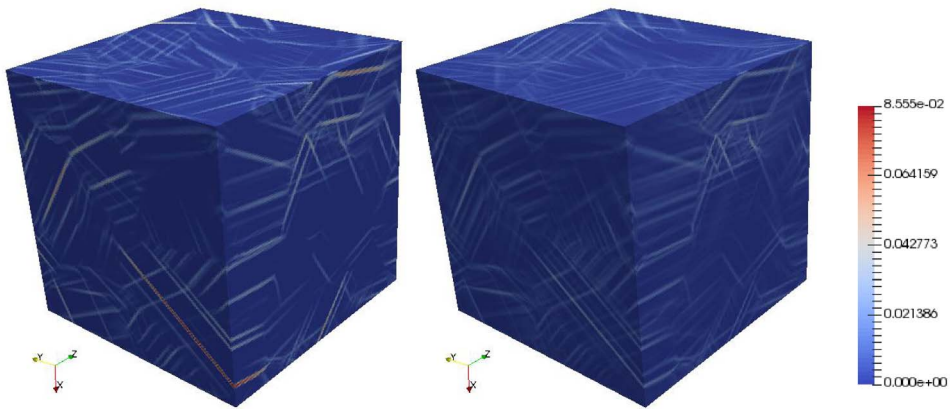


Figure 8. Polycrystal unit-cell—Cumulated plastic strain fields (at 0.2% macroscopic plastic strain), for two grain sizes $D_g = 1 \mu\text{m}$ (left) and $D_g = 100 \mu\text{m}$ (right), with $n_x = 50$ for both simulations. Colorbar is adjusted to the data range of the case ($D_g = 1 \mu\text{m}$).

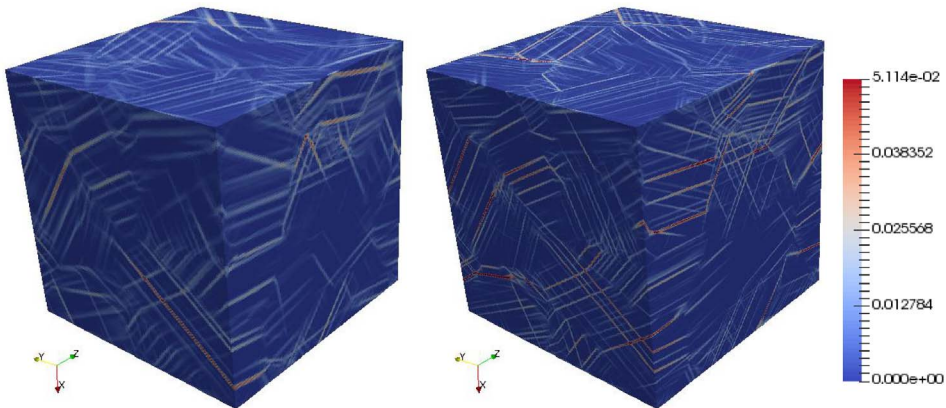


Figure 9. Polycrystal unit-cell—Cumulated plastic strain fields (at 0.2% macroscopic plastic strain), for two layer thicknesses ($e = 2\delta x = 2D_g/n_x$, with $D_g = 10 \mu\text{m}$) associated to two grid refinements ($n_x = 50$, left) and ($n_x = 100$, right). Colorbar is adjusted to the data range of the case ($n_x = 50$).

grain size, the higher the number of activated layers and the lower the heterogeneity. To explain this result, it must be kept in mind that with the choice $e = 2\delta x$ made for the simulations, for a given refinement (here $n_x = 50$), the layer thickness is proportional to the grain size ($e = 2D_g/n_x$). Hence, the volume of the layers, V_{layer} , taken into account in the Weibull model (Equations (1) and (2)) to define the random CRSS, linearly depends on D_g^3 . As the standard deviation is proportional to $V_{\text{layer}}^{-1/m}$ (see Section 2), the CRSS fields are less heterogeneous when increasing the grain size D_g , and, consequently, additional layers can be activated and the plastic strain heterogeneity is reduced. Note that in the extreme case $D_g \rightarrow \infty$, the mean, the median and the standard deviation of τ_s^f , tend to 0 and the CRSS field tends towards a homogeneous field τ_P (see (5)) resulting in a plastic strain field similar to Figure 7 (left).

The influence of the layer thickness is reported in Figure 9. With the choice $e = 2\delta x$, the two grid refinements ($n_x = 50$ and $n_x = 100$) correspond to two layer thicknesses. The thinner

the layer thickness, the higher the heterogeneity. A simple geometrical explanation could be proposed. For a given number of activated layers in the two simulations, there is a factor of two when considering their volume fractions. Hence, for a given macroscopic plastic strain (e.g. 0.2%), the average plastic strain in the activated layer will be higher for the highest refinement.

6. Discussions

The present model extends the initial purpose of “smooth” classical continuum-based CP to less “smooth” applications. It is justified by the limitations of classical CP to reproduce experiment at the micron scale, such as the stochastic results observed on micropillars or intense intragranular plastic strain localization (slip bands) observed on polycrystals. From the mechanisms point of view, the stochastic distribution of CRSS is justified by the statistical distribution of dislocation sources. Of course, the description remains rather simple but it can be regarded as a simple way to account for micro-plasticity in polycrystalline simulations. The fine details associated to the description of intermittent plasticity are not taken into account but signs of microplasticity are reproduced. From the macroscopic point of view, Figure 5 reveals that the first signs of plasticity (square symbols) appear very early when compared to $\sigma_{0.2\%}^y$ (circle symbols). This difference is associated to the successive activation of slip band (layers) in the grains. The macroscopic plastic flow becomes important as soon as a sufficient amount of bands are activated in the polycrystal. This description of intra-granular plastic strain fields exhibiting intense plastic slip bands is also in qualitative agreement with experimental observations of slip bands observed during the micro-plasticity regime, which are not reproduced by conventional CP.

In Section 3.2.3, the m exponent is chosen so that the CRSS distribution lying in samples of volume $V = D^3$ follow a sample size dependence $D^{-0.5}$. These distributions are directly linked (through the geometrical Schmid factor) to the distribution of yield stresses obtained on single crystalline samples, independently submitted to a uniform stress. Introducing the stochastic distribution of CRSS in the different layers of the polycrystal generates a very complex microstructure giving rise to complex grain-to-grain interactions and leading to the macroscopic yield stress of the polycrystal $\sigma_{0.2\%}^y$ as a homogenization result. Hence, if the grain size dependence $D_g^{-0.5}$ deduced from the numerical simulation appears intuitive as we introduced a CRSS sample size dependence $D^{-0.5}$, it was forgetting the fact that the macroscopic yield stress results from a homogenization procedure on a rather complex microstructure. In addition, the Weibull exponent used here is a realistic exponent with respect to experiment (micropillar) and in that sense, the grain size dependence of the macroscopic yield stress resulting from the present approach can be regarded as “predictive”.

The hardening effects arising from dislocation interactions are not considered in this first attempt to account for stochastic CRSS distributions. This approximation is probably valid as soon as the plastic strains remains small. However, a direct use in each voxel of a dislocation-based hardening CP law could be considered without any technical (implementation) issue. In that case, interactions associated to latent hardening will be possible if and only if the two systems are activated in a same voxel. Hence, latent hardening will be active in:

- the voxels of a same layer if two slip systems are activated. In such layers, the interactions between coplanar systems will be taken into account
- the voxels at the intersection of two different layers with at least one activated slip per layer. In such intersecting domains, interactions between non co-planar systems will be taken into account.

7. Conclusion and future prospects

The present approach combining a random distribution of CRSS with layered crystal plasticity is an efficient way to introduce grain size effects in 3D numerical simulations. It is an extension to 3D CP-FFT (or FEM) simulations of dislocation dynamics simulations, performed on single crystal micropillars, with a dislocation source length distribution explaining the sample size effect on the yield stress [20]. Actually, the random CRSS fields are generated from a random distribution of sources regarded as a random Poisson point process in space and strength. Assigning the minimum source strength within a layer to the whole layer, plasticity propagates easily but, as a counterpart, the position of the weakest source is lost. Macroscopically, a Hall-Petch like relationship is adjusted from the simulated yield stresses. The conventional yield stress $\sigma_{0.2\%}^y$, is very different from $\sigma_{0\%}^y$ detecting the first sign of plasticity, revealing an important microplasticity (local plasticity while the macroscopic behaviour remains almost elastic). In addition, it is remarkable that the macroscopic variability observed on the single crystal unit-cell completely vanishes with the 27 grains polycrystal unit-cell.

The present approach allows to better reproduce, at least qualitatively, the experimental observations of plastic strain localizations associated to slip traces at the grains surface, extremely pronounced in irradiated polycrystals but also observed in many unirradiated metals. As a future prospect, a deeper analysis of the strain fields will have to be performed to evaluate quantities that could be compared to experiment such as the band spacing or the number of band orientations per grain.

An open question coming with the per layer CRSS distribution is the choice of the layer thickness. Actually, the spatial distribution of sources within a layer cannot be taken into account (as observed in Section 4.1 with the per voxel distribution of CRSS). This point becomes a problem as soon as the stress becomes heterogeneous so that in the polycrystal, for a given grain size, reducing the layer thickness increases the yield stress. Improving this point is still under investigation. The value of the layer thickness could be associated to experimental measurements of slip localization bands (e.g. in irradiated materials [30]). Then, the effect of the ratio $e/\delta x$, assumed constant (i.e. 2) along the paper, was studied in a previous paper dealing with a unique slip plane (basal plane for hexagonal irradiated zirconium) [12]. The results were not completely converged with $e/\delta x = 2$ but the use of composite voxels drastically improved this point. Adapting the idea of composite voxels, here with four {111} slip planes, could be a future prospect. However, note that introducing a hardening term to the CP law could also reduce this effect.

Finally, for the sake of simplicity and to separate the different hardening sources, the present approach was proposed with a very simple quasi-perfect crystal plasticity law. Hence, all the hardening behaviour, from the early onset of plasticity ($\sigma_{0\%}^y$) to 1% plastic strain ($\sigma_{1\%}^y$) consists of a kinematic hardening induced by the strong plastic strain localization. The next step will be to introduce dislocation densities and their interactions to complement the behaviour with an isotropic hardening contribution.

Acknowledgements

The author acknowledges Etienne Castelier from CEA for fruitful discussions on Poisson point processes and the weakest link Weibull modelling.

The work was funded by CEA through the MATIX project within the SIMU program.

References

- [1] G. Monnet, L. Vincent, L. Gélébart, "Multiscale modeling of crystal plasticity in reactor pressure vessel steels: Prediction of irradiation hardening", *J. Nucl. Mater.* **514** (2019), p. 128-138.

- [2] G. Venkatramani, S. Ghosh, M. Mills, “A size-dependent crystal plasticity finite-element model for creep and load shedding in polycrystalline titanium alloys”, *Acta Mater.* **55** (2007), no. 11, p. 3971-3986.
- [3] R. A. Rubio, S. Haouala, J. LLorca, “Grain boundary strengthening of fcc polycrystals”, *J. Mater. Res.* **34** (2019), no. 13, p. 2263-2274.
- [4] M. E. Gurtin, “A gradient theory of single-crystal viscoplasticity that accounts for geometrically necessary dislocations”, *J. Mech. Phys. Solids* **50** (2002), no. 1, p. 5-32.
- [5] A. Acharya, A. Roy, “Size effects and idealized dislocation microstructure at small scales: Predictions of a phenomenological model of mesoscopic field dislocation mechanics: Part I”, *J. Mech. Phys. Solids* **54** (2006), no. 8, p. 1687-1710.
- [6] S. Berbenni, V. Taupin, R. A. Lebensohn, “A fast fourier transform-based mesoscale field dislocation mechanics study of grain size effects and reversible plasticity in polycrystals”, *J. Mech. Phys. Solids* **135** (2020), article no. 103808.
- [7] S. Haouala, S. Lucarini, J. LLorca, J. Segurado, “Simulation of the Hall–Petch effect in fcc polycrystals by means of strain gradient crystal plasticity and fft homogenization”, *J. Mech. Phys. Solids* **134** (2020), article no. 103755.
- [8] P. Franciosi, L. T. Le, G. Monnet, C. Kahloun, M.-H. Chavanne, “Investigation of slip system activity in iron at room temperature by sem and afm in-situ tensile and compression tests of iron single crystals”, *Int. J. Plast.* **65** (2015), p. 226-249.
- [9] F. D. Gioacchino, J. Q. da Fonseca, “An experimental study of the polycrystalline plasticity of austenitic stainless steel”, *Int. J. Plast.* **74** (2015), p. 92-109.
- [10] F. Bourdin, J. C. Stinville, M. P. Echlin, P. G. Callahan, W. C. Lenthe, C. J. Torbet, D. Texier, F. Bridier, J. Cormier, P. Villechaise, T. M. Pollock, V. Valle, “Measurements of plastic localization by heaviside-digital image correlation”, *Acta Mater.* **157** (2018), p. 307-325.
- [11] A. Marano, L. Gélébart, S. Forest, “Intragranular localization induced by softening crystal plasticity: Analysis of slip and kink bands localization modes from high resolution fft-simulations results”, *Acta Mater.* **175** (2019), p. 262-275.
- [12] A. Marano, L. Gélébart, “Non-linear composite voxels for fft-based explicit modeling of slip bands: Application to basal channeling in irradiated zr alloys”, *Int. J. Solids Struct.* **198** (2020), p. 110-125.
- [13] A. Patra, D. L. McDowell, “Crystal plasticity investigation of the microstructural factors influencing dislocation channeling in a model irradiated bcc material”, *Acta Mater.* **110** (2016), p. 364-376.
- [14] A. Marano, “Numerical simulation of strain localization in irradiated polycrystals”, PhD Thesis, Université PSL, CEA Paris-Saclay & MINES ParisTech, 2019.
- [15] M. Zhang, F. Bridier, P. Villechaise, J. Mendez, D. L. McDowell, “Simulation of slip band evolution in duplex ti–6al–4v”, *Acta Mater.* **58** (2010), no. 3, p. 1087-1096.
- [16] S. Papanikolaou, Y. Cui, N. Ghoniem, “Avalanches and plastic flow in crystal plasticity: an overview”, *Model. Simul. Mat. Sci. Eng.* **26** (2017), no. 1, article no. 013001.
- [17] P. M. Derlet, R. Maafs, “A probabilistic explanation for the size-effect in crystal plasticity”, *Philos. Mag.* **95** (2015), no. 16-18, p. 1829-1844.
- [18] P. S. Phani, K. E. Johanns, E. P. George, G. M. Pharr, “A simple stochastic model for yielding in specimens with limited number of dislocations”, *Acta Mater.* **61** (2013), no. 7, p. 2489-2499.
- [19] P. D. Ispánovity, Á. Hegyi, I. Groma, G. Györgyi, K. Ratter, D. Weygand, “Average yielding and weakest link statistics in micron-scale plasticity”, *Acta Mater.* **61** (2013), no. 16, p. 6234-6245.
- [20] J. A. El-Awady, M. Wen, N. M. Ghoniem, “The role of the weakest-link mechanism in controlling the plasticity of micropillars”, *J. Mech. Phys. Solids* **57** (2009), no. 1, p. 32-50.
- [21] S. Shao, N. Abdolrahim, D. F. Bahr, G. Lin, H. M. Zbib, “Stochastic effects in plasticity in small volumes”, *Int. J. Plast.* **52** (2014), p. 117-132, In Honor of Hussein Zbib.
- [22] E. Castelner, L. Gélébart, C. Lacour, C. Lantuejoul, “Three consistent approaches of the multiple cracking process in 1d composites”, *Compos. Sci. Technol.* **70** (2010), no. 15, p. 2146-2153.
- [23] R. Y. Rubinstein, *Simulation and the Monte Carlo Method*, 1st ed., John Wiley & Sons, Inc., USA, 1981.
- [24] L. Gelebart, J. Derouillat, N. Doucet, F. Ouaki, A. Marano, J. Duverge, “Amitex_FFFTP”, 2020, http://www.maisondelasimulation.fr/projects/amitex/general/_build/html/index.html.
- [25] M. Schneider, D. Merkert, M. Kabel, “Fft-based homogenization for microstructures discretized by linear hexahedral elements”, *Int. J. Numer. Methods Eng.* **109** (2017), no. 10, p. 1461-1489.
- [26] T. Helfer, B. Michel, J.-M. Proix, M. Salvo, J. Sercombe, M. Casella, “Introducing the open-source mfront code generator: Application to mechanical behaviours and material knowledge management within the pleiades fuel element modelling platform”, *Comput. Math. Appl.* **70** (2015), no. 5, p. 994-1023.
- [27] Y. Kamimura, K. Edagawa, S. Takeuchi, “Experimental evaluation of the peierls stresses in a variety of crystals and their relation to the crystal structure”, *Acta Mater.* **61** (2013), no. 1, p. 294-309.
- [28] J. Senger, D. Weygand, C. Motz, P. Gumbsch, O. Kraft, “Aspect ratio and stochastic effects in the plasticity of uniformly loaded micrometer-sized specimens”, *Acta Mater.* **59** (2011), no. 8, p. 2937-2947.
- [29] R. J. Asaro, J. R. Rice, “Strain localization in ductile single crystals”, *J. Mech. Phys. Solids* **25** (1977), no. 5, p. 309-338.

- [30] F. Onimus, I. Monnet, J. Béchade, C. Prioul, P. Pilvin, “A statistical tem investigation of dislocation channeling mechanism in neutron irradiated zirconium alloys”, *J. Nucl. Mater.* **328** (2004), no. 2, p. 165-179.